# Electron energy spectrum and density of states for nonsymmetric semiconductor heterostructures in an in-plane magnetic field

A. Hernández-Cabrera* and P. Aceituno
*Departamento Física Básica, Universidad de La Laguna, La Laguna, 38206-Tenerife, Spain*

F. T. Vasko†
*Institute of Semiconductor Physics, NAS Ukraine, Prospekt Nauki 41, Kiev, 03028, Ukraine*
(Received 21 March 2006; revised manuscript received 25 May 2006; published 24 July 2006)

Modifications of spin-splitting dispersion relations and density of states for electrons in nonsymmetric heterostructures under in-plane magnetic field are studied within the envelope function formalism. Spin-orbit interactions, caused by both a slow external potential and the heterojunction potentials (which are described by the boundary conditions) are taken into account. The interplay between these contributions and the magnetic field contribution to the spin-splitting term in the Hamiltonian is essential when energy amounts resulting from the Zeeman and spin-orbit coupling are of the same order. Such modifications of the energy spectra allow us to separate the spin-orbit splitting contributions due to a slow external potential and due to the heterojunctions. Numerical estimates for a selectively doped heterojunction and quantum well with a narrow-gap region of electron localization are performed.

DOI: 10.1103/PhysRevB.74.035330 PACS number(s): 73.21.−b, 72.25.−b

## I. INTRODUCTION

Spin-orbit splitting of the energy dispersion relations for electrons in nonsymmetric quantum heterostructures has been theoretically considered during the past decades (see Ref. 1 for a review). In bulk materials spin-orbit interaction appears both due to a slow external potential[2] and due to cubic[3] and linear[4] spin-dependent contributions to the effective mass Hamiltonian. Turning to the two-dimensional (2D) case, we can reduce the cubic contribution to a linear one after the replacement of the squared momentum by the quantized value due to confinement.[5] It is still more important the fact that we have to take into account an additional spin-orbit splitting of the energy spectrum due to the interaction with abrupt heterojunction potentials (see Ref. 6 and discussion in Refs. 1 and 7). Such contribution is of a radically different kind with respect to that listed above because contributions from both sides of a slow confinement potential compensate each other[8] and, therefore, the spin-splitting of 2D states cannot be obtained without a short-range potential contribution. To the best of our knowledge, the relative contributions from the bulk-induced mechanisms[2–4] and from the heterojunctions have not been clarified experimentally in spite of a set of existing theoretical calculations.[1] In this paper we have examined the effect of an in-plane magnetic field on the electron energy spectrum and density of states and we have found that magnetoinduced modifications of these characteristics are essentially different from the 2D spin-orbit interaction and Zeeman splitting. In principle, this fact makes possible an experimental verification of the above discussed contributions of the spin-orbit interaction.

The effect of in-plane magnetic field on the energy spectrum in nonsymmetric heterostructures occurs due to the Zeeman term in the electron Hamiltonian. This fact has been found in Ref. 9, shortly after initial considerations of the spin-orbit splitting in nonsymmetric heterostructures (see Refs. 1, 10, and 11). A number of peculiarities in transport phenomena for 2D systems under an in-plane magnetic field were also discussed[11–13] and more complicated cases, such as quasi-1D transport or spin Hall effect (see references in Refs. 14 or 15, respectively) were recently considered. All this papers only take into account the mix between the Zeeman contribution and the effective 2D spin-orbit interaction. Here we perform the calculations based on the three-band Kane model[16] with nonsymmetric boundary conditions at abrupt heterojunctions, which is valid for narrow-gap heterostructures, and with a slow external potential. The analysis of magnetoinduced modifications of 2D energy spectra and corresponding density of states is presented for typical parameters of InGaAs/InAlAs-selectively doped heterojunctions, and for the undoped InGaAs- or InSb-based quantum wells (QWs). Typical band diagrams are shown in Figs. 1(a) and 1(b). We have used self-consistent calculations for selectively doped structures [Fig. 1(a)] while QWs are subjected to a homogeneous electric field [Fig. 1(b)]. Note that the spin-orbit splitting in selectively doped heterojunctions is analyzed from the Shubnikov-de Haas (SdH)

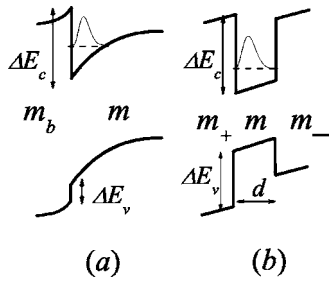


FIG. 1. Band diagrams for the selectivly doped $In_{0.75}Al_{0.25}As/In_{0.75}Ga_{0.25}As$ heterojunction (a) and for the InGaAs/InAlAs quantum well (b). Dashed lines show electron ground state energy levels and thin curves correspond to wave functions; $d$ is the QW's width, $\Delta E_{c,v}$ are the band offsets, and $m$ is the effective mass in the narrow-gap region, while $m_b$ and $m_\pm$ are the barrier effective masses.

 

oscillations,[12,13] while peculiarities of the density of states in the undoped narrow-gap QWs can be directly observed with the use of the mid-ir photoluminescence excitation (PLE) measurements.

The paper is organized as follows. In the next section we discuss the conduction $c$-band eigenstate problem and describe the electronic states in nonsymmetric narrow-gap heterostructures using the boundary conditions for the wave functions at the interfaces in the parabolic approximation. In Sec. III we solve the 2D-eigenstate problem using the averaged transverse field approach. Numerical self-consistent calculations of the magnetoinduced (caused by a magnetic field) modifications of the energy spectra and the density of states are presented in Sec. IV. Conclusions are given in the last section.

## II. BASIC EQUATIONS

We start from the formulation of the eigenstate problem for the electronic state of the conduction $c$-band localized in the selectively doped heterojunction or in the nonsymmetric QW. All the above listed spin-dependent contributions are taken into account in the analysis. We also present the density of states which is connected to the PLE intensity.

### A. Three-band Kane model

The electronic states in narrow-gap heterostructures are described by the three-band Kane matrix Hamiltonian[16]

$$\hat{\varepsilon}_z + (\hat{\mathbf{v}} \cdot \hat{\boldsymbol{\pi}}), \quad \hat{\boldsymbol{\pi}} = \hat{\mathbf{p}} - \frac{e}{c}\mathbf{A}, \tag{1}$$

where the kinetic momentum, $\hat{\boldsymbol{\pi}}$, contains the vector potential $\mathbf{A}=(Hz,0,0)$, $\mathbf{H}\|OY$ is an in-plane magnetic field and $\hat{\mathbf{p}}=(\mathbf{p},\hat{p}_z)$ is written in the $\mathbf{p}$, $z$-representation through the 2D momentum $\mathbf{p}$. Here we have also introduced the diagonal energy matrix $\hat{\varepsilon}_z$ whose elements determine the positions of the band extrema (the energy values $\varepsilon_{cz}$, $\varepsilon_{hz}$, and $\varepsilon_{lz}$ correspond to electron, heavy-, and light-hole extrema) and the interband velocity matrix $\hat{\mathbf{v}}$. The $6\times 6$ Hermitian matrix $\hat{\mathbf{v}}$ is determined by the following nonzero matrix elements:[7]

$$v^x_{13} = v^x_{26} = \mathcal{P}/\sqrt{2}, \quad v^x_{15} = -v^x_{24} = -\mathcal{P}/\sqrt{6},$$

$$v^y_{13} = -v^y_{26} = -i\mathcal{P}/\sqrt{2}, \quad v^y_{15} = v^y_{24} = -i\mathcal{P}/\sqrt{6},$$

$$v^z_{14} = v^z_{25} = \sqrt{2/3}\mathcal{P}, \tag{2}$$

and $\mathcal{P}$ is the characteristic interband velocity for the Kane model.

Neglecting the small contributions from other bands we suppose in Eq. (1) that the inverse heavy hole effective mass is equal to zero. For such a case valence $v$-band components of the wave functions, $\psi^{(3-6)}_{\mathbf{p}z}$, are expressed in terms of the $c$-band spinor with components $\psi^{(1,2)}_{\mathbf{p}z}$ and the effective Schrödinger equation for this spinor takes the form (see Ref. 17 where the case $H=0$ has been considered)

$$\left\{ \varepsilon_{cz} - E - \frac{2}{3}\mathcal{P}^2\left( \frac{\pi_+\pi_-}{\varepsilon_{vz}-E} + \hat{p}_z[\varepsilon_{vz}-E]^{-1}\hat{p}_z \right) + \begin{bmatrix} 0 & \left[\frac{\pi_+}{\varepsilon_{vz}-E}, \hat{p}_z\right] \\ -\left[\frac{\pi_-}{\varepsilon_{vz}-E}, \hat{p}_z\right] & 0 \end{bmatrix} \right\} \begin{bmatrix} \psi^{(1)}_{\mathbf{p}z} \\ \psi^{(2)}_{\mathbf{p}z} \end{bmatrix} = 0, \tag{3}$$

where $\pi_\pm = (\pi_x \pm i\pi_y)$ are the circular components of the in-plane momenta. For the sake of simplicity we have neglected here the strain effect due to lattice mismatch[18] and used $\varepsilon_{vz} \equiv \varepsilon_{hz} = \varepsilon_{lz}$. It is convenient to introduce in Eq. (3) the $z$-dependent effective mass, $m_z$, the characteristic spin velocity, $V_z$, and the effective $g$-factor, $g_z$, according to the relations:

$$m_z = -\frac{3}{4\mathcal{P}^2}(\varepsilon_{vz}-E), \quad V_z = \frac{\hbar}{4m_z}\frac{(d\varepsilon_{vz}/dz)}{\varepsilon_{vz}-E},$$

$$g_z = \frac{m_e}{2m_z}\left[1 - z\frac{(d\varepsilon_{vz}/dz)}{\varepsilon_{vz}-E}\right]. \tag{4}$$

In such definitions Eq. (3) may be rewritten as the spinor eigenvalue problem:

$$\left\{ \varepsilon_{cz} - E + \frac{(p_x - eHz/c)^2 + p_y^2}{2m_z} + \hat{p}_z\frac{1}{2m_z}\hat{p}_z - V_z[\hat{\boldsymbol{\sigma}} \times \mathbf{p}]_z + \frac{g_z}{2}\mu_B H\hat{\sigma}_y \right\} \Psi_{\mathbf{p}z} = 0, \tag{5}$$

where spinor $\Psi_{\mathbf{p}z}$ is determined by the components $\psi^{(1,2)}_{\mathbf{p}z}$, $\mu_B \equiv |e|\hbar/(m_e c)$ is the Bohr magneton, and $\hat{\boldsymbol{\sigma}}$ is the Pauli matrix. The energy values of $c$- and $v$-band extrema for the narrow-gap ($A$) and wide-gap ($B$) regions take the forms

$$\varepsilon_{cz} = U_z, \quad \varepsilon_{vz} = -\varepsilon_g + U_z, \quad (A)$$

$$\varepsilon_{cz} = \Delta E_c + U_z, \quad \varepsilon_{vz} = -\varepsilon_g + \Delta E_v + U_z, \quad (B) \tag{6}$$

and the corresponding band diagrams for a QW and selectively doped heterojunction are shown in Fig. 1. Here the energy is counted from the bottom of the $c$-band, $\varepsilon_g$ is the gap, and $\Delta E_c$ and $\Delta E_v$ are the band offsets for $c$- and $v$-bands, correspondingly. Here the slow external potential $U_z$ should be determined from a self-consistent procedure. Thus, after substitution of Eq. (6) in Eq. (5) we have formulated the eigenstate problem for the spinor $\Psi_{\mathbf{p}z}$.

Since $\Delta E_c \geqslant \varepsilon_g$ in narrow-gap heterostructures, then the weak underbarrier penetration of wave function takes place for the electronic states with $E \ll \varepsilon_g$ (parabolic band approximation). Because of this, one can neglect the longitudinal motion for the underbarrier region, $z<0$ for the single heterojunction case shown in Fig. 1(a), where the solutions take the form

$$\Psi_{\mathbf{p}z} \simeq \Psi_{\mathbf{p}z=0} e^{\kappa z}, \quad z<0. \tag{7}$$

Here $\hbar\kappa=\sqrt{2m_b\Delta E_c}$ and $\kappa^{-1}$ determines the scale of the underbarrier penetration of wave functions. We have also used in Eq. (7) the continuity conditions for eigenfunctions $\Psi_{\mathbf{p}z}$ at heterojunctions. Since $V_z$ in Eq. (4) is proportional to $(d\varepsilon_{vz}/dz)$, then the integration (5) over heterojunction produces additional contributions to the boundary condition for flows. Such contributions are proportional to the band offset at the heterojunction $\Delta E_v$. Eliminating the underbarrier contributions from such equation by the use of the explicit expression (7) we obtain the third kind boundary conditions:[6,7]

$$(\hat{p}_z\Psi_{\mathbf{p}z})|_{z=0} - iP_o\Psi_{\mathbf{p}z=0} - i\chi[\hat{\boldsymbol{\sigma}}\times\mathbf{p}]_z\Psi_{\mathbf{p}z=0} = 0. \tag{8}$$

Here the momenta $P_o=\hbar\kappa m/m_b$ characterizes the underbarrier penetration and the parameter $\chi$ determines the spin-orbit coupling due to the abrupt potential of the heterojunction

$$\chi = \frac{2m_b}{\hbar}\int_{-\delta}^{\delta} dz V_z \simeq \frac{\Delta E_v}{2\varepsilon_g} \tag{9}$$

and the right-side part is written for the approximation $m_b \simeq m$.

### B. Eigenstate problem

In the parabolic approximation, we describe the $c$-band electronic states using the above introduced spinor $\Psi_{\mathbf{p}z}$. Below we consider not very strong magnetic fields, $\hbar\omega_c \ll \bar{v}\hbar/\bar{d}$, where $\omega_c$ is the cyclotron frequency, $\bar{v}$ and $\bar{d}$ are the characteristic velocity and width, when $(p_x-eHz/c)^2$ in Eq. (5) is replaced by $p_x^2$ and the isotropic kinetic energy is given by $\varepsilon_p \equiv (p_x^2+p_y^2)/(2m)$ and includes the effective mass $m$. Considering the low energy region (if $\varepsilon_g \gg \bar{\varepsilon}$) we rewrite the Schrödinger equation (5) for the narrow-gap region in the form

$$\left(\varepsilon_p + \frac{\hat{p}_z^2}{2m} + U_z + \hat{W}_z\right)\Psi_{\mathbf{p}z} = E\Psi_{\mathbf{p}z},$$

$$\hat{W}_z = -V_z[\hat{\boldsymbol{\sigma}}\times\mathbf{p}]_z + \frac{g_z}{2}\mu_B H\hat{\sigma}_y, \tag{10}$$

where $U_z$ is the self-consistent potential, as given in Eq. (14) below, and the effective mass is $z$-independent. The spin velocity $V_z$ and the $z$-dependent contribution to the $g$-factor are proportional to the transverse electric field $dU_z/dz$:

$$V_z \simeq -\frac{\hbar}{4m\varepsilon_g}\frac{dU_z}{dz}, \quad g_z \simeq \frac{m_e}{2m}\left(1+\frac{z}{\varepsilon_g}\frac{dU_z}{dz}\right). \tag{11}$$

For the selectively doped heterojunction case we consider Eq. (10) for the $z>0$ region with the boundary conditions (8) and with $\Psi_{\mathbf{p}z\to\infty}=0$. For the case of a QW of width $d$, one can eliminate the underbarrier contributions in analogy to Eqs. (7)–(9) and, in addition to Eq. (10) for the region $|z|<d/2$, the following third kind boundary conditions should be used

$$(\hat{p}_z\Psi_{\mathbf{p}z})|_{z=\pm d/2} \mp iP_\pm\Psi_{\mathbf{p},\pm d/2} + i\chi_\pm[\hat{\boldsymbol{\sigma}}\times\mathbf{p}]_z\Psi_{\mathbf{p},\pm d/2} = 0. \tag{12}$$

Here momenta $P_\pm=\sqrt{2m_\pm\Delta E_\pm}(m/m_\pm)$ determine the scale of the underbarrier penetration of wave functions; the different values of $\Delta E_\pm$ and $m_\pm$ take into account the differences of band offsets and effective masses, as it is shown in Fig. 1(b). The parameters $\chi_\pm \simeq \Delta E_v/2\varepsilon_g$ determine the spin-orbit coupling due to the abrupt potential of the heterojunction according to Eq. (9). When $m_+=m_-$, which corresponds to the symmetric case, we will take $P_\pm=P_o$ and $\chi_\pm=\chi$, as we can see from Eq. (9).

Thus both interface potentials, which determine the spin-dependent contributions to Eq. (12), and the intrawell field, which determines the spin velocity $V_z$ in Eq. (11), are responsible for the spin-splitting of energy spectra. Since the Zeeman spin-splitting term only appears in Eq. (10), the mentioned magnetoinduced modifications of electron states due to these two contributions are different.

In the case of selectively doped structures, the self-consistent numerical procedure for the eigenstate problem (10) involves the potential $U_z$, which is obtained from the Poisson equation in the following form:

$$U_z = \frac{4\pi e^2}{\epsilon}\int_{-\infty}^{z} dz'(z-z')[n_D(z') - n_e(z')]. \tag{13}$$

Here $n_D(z)$ is the 3D concentration of donors and $\epsilon$ is the dielectric permittivity that we have supposed as uniform across the heterostructure. The electron density distribution is introduced through the electron dispersion relations $E_{\sigma\mathbf{p}}$ according to

$$n_e(z) = \sum_\sigma \int \frac{d\mathbf{p}}{(2\pi\hbar)^2}\Psi_{\mathbf{p}z}^{(\sigma)+}\cdot\Psi_{\mathbf{p}z}^{(\sigma)}\theta(\varepsilon_F - E_{\sigma\mathbf{p}}), \tag{14}$$

where $\Psi_{\mathbf{p}z}^{(\sigma)+}$ denotes the Hermitian conjugate of $\Psi_{\mathbf{p}z}^{(\sigma)}$ and $\sigma=\pm 1$ refers to the two possible spin orientations. The Heaviside function, $\theta(x)$, appears here for the zero-temperature case. The Fermi energy, $\varepsilon_F$, is expressed through the total electron density, $n_{2D}$, defined as $n_{2D}=\int dz n_e(z)$. Thus $\varepsilon_F$ depends on $H$ for the fixed concentration case.

The density of states is given by the standard formula

$$\rho_\varepsilon = \sum_\sigma \int \frac{d\mathbf{p}}{(2\pi\hbar)^2}\delta(\varepsilon - E_{\sigma\mathbf{p}}). \tag{15}$$

In order to analyze $\rho_\varepsilon$ one needs to solve the above-formulated eigenstate problem and to perform the integrations in Eq. (15). The density of states is connected to PLE intensity for the case of near-edge transitions, $I_{PLE}$. Since the interband matrix element $\mathbf{v}_{cv}$ does not depend on the in-plane quantum numbers, one obtains:[7,19]

$$I_{PLE} \sim \sum_{\lambda_c\lambda_v} |\mathbf{e}\cdot\mathbf{v}_{cv}|^2\delta(\varepsilon_{\lambda_c} - \varepsilon_{\lambda_v} - \hbar\omega) \sim \rho_{\hbar\Delta\omega}, \tag{16}$$

where $\mathbf{e}$ is the polarization vector, $\Delta\omega=\omega-\bar{\varepsilon}_g/\hbar$, and $\bar{\varepsilon}_g$ is the gap energy, which is renormalized due to the confinement effect.

## III. ANALYTICAL CONSIDERATION

Before the numerical consideration we perform a simplified calculation of the eigenstate problem using the uniform transverse field approximation $U_z \simeq eF_\perp z$ which is valid for nondoped QWs under an external modulating field $F_\perp$; for heavy-doped structures $F_\perp$ implies an averaged self-consistent transverse field.

### A. Average field approach

A simplification of the eigenstate problem (10) appears due to the $z$-independent spin-orbit perturbation when $\hat{W}_z$ in Eq. (10) becomes

$$\hat{W} = \bar{v}[\hat{\boldsymbol{\sigma}} \times \mathbf{p}]_z + w_H \hat{\sigma}_y \tag{17}$$

with the averaged across structure characteristic spin velocity $\bar{v} \simeq |e|F_\perp \hbar/(4m\varepsilon_g)$ and the Zeeman splitting $w_H = (\bar{g}/2)\mu_B H$, where the $z$-dependent correction to the $g$-factor is neglected. The fundamental solutions $\Psi_{\mathbf{p}z}$ for Eq. (10), with the spin-dependent contribution (17), can be factorized as products of functions $\Psi_{\mathbf{p}}^{(\sigma)}$ and $\varphi_z^{(k\sigma)}$. Here the spinors $\Psi_{\mathbf{p}}^{(\sigma)}$ for $\sigma = \pm 1$ are determined from the eigenstate problem:

$$(\varepsilon_p + \hat{W})\Psi_{\mathbf{p}}^{(\sigma)} = \varepsilon_{\sigma\mathbf{p}} \Psi_{\mathbf{p}}^{(\sigma)}, \tag{18}$$

whose solutions are given[10] by

$$\Psi_{\mathbf{p}}^{(+1)} = \frac{1}{\sqrt{2}} \begin{bmatrix} 1 \\ (\bar{v}p_+ + w_H)/iw_{\mathbf{p}} \end{bmatrix},$$

$$\Psi_{\mathbf{p}}^{(-1)} = \frac{1}{\sqrt{2}} \begin{bmatrix} (\bar{v}p_- + w_H)/iw_{\mathbf{p}} \\ 1 \end{bmatrix},$$

$$\varepsilon_{\sigma\mathbf{p}} = \varepsilon_p + \sigma w_{\mathbf{p}}, \quad w_{\mathbf{p}} = \sqrt{(\bar{v}p_x + w_H)^2 + (\bar{v}p_y)^2}, \tag{19}$$

where $p_\pm = p_x \pm ip_y$ and the energy values $\varepsilon_{\pm\mathbf{p}}$ describe the mix between internal spin-orbit interaction and Zeeman spin splitting.

The two $z$-dependent fundamental solutions $\varphi_z^{(k\sigma)}$ (labeled below by $k = a, b$) are determined from the equation

$$\left(\frac{\hat{p}_z^2}{2m} + eF_\perp z\right)\varphi_z^{(k\sigma)} = (E - \varepsilon_{\sigma\mathbf{p}})\varphi_z^{(k\sigma)}, \tag{20}$$

written for the narrow-gap region.

The general spinor solution $\Psi_{\mathbf{p}z}$ is expressed through these fundamental solutions according to

$$\Psi_{\mathbf{p}z} = \Psi_{\mathbf{p}}^{(+1)}(A_+\varphi_z^{(a,+1)} + B_+\varphi_z^{(b,+1)}) + \Psi_{\mathbf{p}}^{(-1)}(A_-\varphi_z^{(a,-1)} + B_-\varphi_z^{(b,-1)}), \tag{21}$$

where the coefficients $A_\pm, B_\pm$ are determined from the boundary conditions (12) or from Eq. (8) and the requirements $\Psi_{\mathbf{p}z\to\infty} = 0$.

After the substitution of the solution (21) for $\varphi_z^{(b\sigma)} = 0$, which corresponds to the boundary condition at $z \to \infty$, into Eq. (8) and the multiplication of this system by $\Psi_{\mathbf{p}}^{(\sigma)}$ on the left side we rewrite the boundary condition at $z = 0$ as follows:

$$\mathcal{P}_+ A_+ + \chi \Psi_{\mathbf{p}}^{(+1)+} \begin{bmatrix} 0 & -p_+ \\ p_- & 0 \end{bmatrix} \Psi_{\mathbf{p}z=0} = 0,$$

$$\mathcal{P}_- A_- + \chi \Psi_{\mathbf{p}}^{(-1)+} \begin{bmatrix} 0 & -p_+ \\ p_- & 0 \end{bmatrix} \Psi_{\mathbf{p}z=0} = 0, \tag{22}$$

with $\mathcal{P}_\pm \equiv (\hat{p}_z + iP_o)\varphi_z^{(a\pm)}|_{z=0}$. In order to calculate the proportional to $\chi$ contributions we use here the solutions of the spin-dependent eigenstate problem (19). Thus Eq. (22) can be transformed with the use of the relations

$$\Psi_{\mathbf{p}}^{(\sigma)+} \begin{bmatrix} 0 & -p_+ \\ p_- & 0 \end{bmatrix} \Psi_{\mathbf{p}}^{(\sigma)} = \sigma \frac{\bar{v}p^2 + w_H p_x}{iw_{\mathbf{p}}},$$

$$\Psi_{\mathbf{p}}^{(\sigma)+} \begin{bmatrix} 0 & -p_+ \\ p_- & 0 \end{bmatrix} \Psi_{\mathbf{p}}^{(-\sigma)} = -i \frac{w_H p_y}{vp_\sigma + \sigma w_H} \tag{23}$$

to a simple linear system for $A_\pm$. The dispersion relation, $E_{\sigma\mathbf{p}}$, is determined from the zero determinant requirement.

A similar transformation of the boundary conditions (12) for QWs, after substitution in Eq. (21), permit us to rewrite the boundary condition at $z = \pm d/2$ in the form

$$(\hat{p}_z \mp iP_\pm)(A_+\varphi_z^{(a,+1)} + B_+\varphi_z^{(b,+1)})|_{z=\pm d/2} + \chi \Psi_{\mathbf{p}}^{(+1)+} \begin{bmatrix} 0 & -p_+ \\ p_- & 0 \end{bmatrix} \Psi_{\mathbf{p},\pm d/2} = 0,$$

$$(\hat{p}_z \mp iP_\pm)(A_-\varphi_z^{(a,-1)} + B_-\varphi_z^{(b,-1)})|_{z=\pm d/2} + \chi \Psi_{\mathbf{p}}^{(-1)+} \begin{bmatrix} 0 & -p_+ \\ p_- & 0 \end{bmatrix} \Psi_{\mathbf{p},\pm d/2} = 0. \tag{24}$$

Thus we have obtained a linear system for $A_\pm$ and $B_\pm$ and, therefore, $E_{\sigma\mathbf{p}}$ is obtained from the solvability condition for this system.

### B. 2D model

First, let us consider the case of a heterostructure without spin-orbit contributions from heterojunctions, $\chi = 0$, when the dispersion relation is given by Eq. (19). For the zero magnetic field case, $w_H = 0$, the energy $w_{\mathbf{p}}$ is replaced by $\bar{v}p$ and $\varepsilon_{\pm\mathbf{p}}$ in Eq. (19) is transformed to the isotropic dispersion relation $\varepsilon_{\sigma p} = \varepsilon_p + \sigma|\bar{v}|p$. For this case the density of states was considered in Ref. 7. If $w_H \neq 0$, the dispersion relation (19) becomes anisotropic as it is shown in Fig. 2(a). We have used in this figure the dimensionless magnetic field $h = w_H/m\bar{v}^2$. In order to represent a general case, valid for any structure, we have also used a dimensionless energy axis.

For the case of the strong magnetic field, when $w_{\mathbf{p}}$ is replaced by $w_H$, the Zeeman splitting effect appears to be dominant in the dispersion relation: $\varepsilon_{\pm p} \simeq \varepsilon_p \pm w_H$. The spin-orbit splitting is mainly manifested as a shift of the dispersion paraboloids towards higher (lower) $p_x$ values for $\sigma = +1(-1)$, respectively. On the other hand, Zeeman splitting is shown as a displacement to higher (lower) energy values depending on $\sigma$. The anisotropy of the dispersion re-

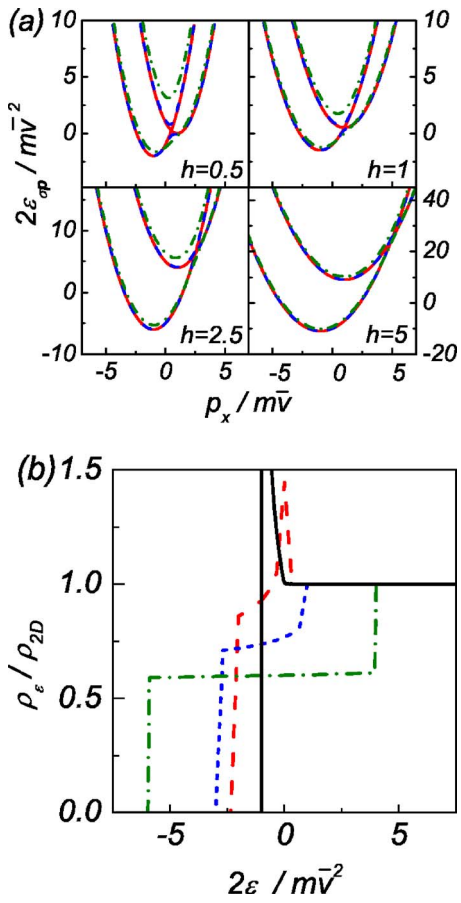


FIG. 2. (Color online) (a) Dispersion laws for different $h$ values. Solid, dashed, and dot-dashed curves corresponds to the dimensionless momenta $p_y/m\bar{v}=0$, 0.25, and 1, respectively. (b) Density of states vs dimensionless energy for magnetic fields $h=0$ (solid), 0.5 (dashed), 1 (dotted), 2.5 (dash-dotted), and 5 (dash-dot-dotted).

lation $\varepsilon_{\sigma\mathbf{p}}$ appears to be essential for the region around the cross-point, $\varepsilon_c \equiv w_H^2/2m\bar{v}^2$.

After the shift $p_x \to p_x - w_H/m\bar{v}$ and the integration over $p$ with the use of the $\delta$ function, the density of states is transformed from Eq. (15) into the integral with respect to the cosine of the in-plane angle, $\zeta=\cos\theta$:

$$\frac{\rho_\varepsilon}{\rho_{2D}} = \frac{1}{2\pi}\sum_\sigma \int_{-1}^{1} \frac{d\zeta}{\sqrt{1-\zeta^2}} \times \frac{\theta(\nu_{\sigma\zeta}^2 - 1 + 2\varepsilon/hw_H)}{\sqrt{\nu_{\sigma\zeta}^2 - 1 + 2\varepsilon/hw_H}} \sum_\pm \mathcal{E}_\pm \theta(\mathcal{E}_\pm). \tag{25}$$

Here $\mathcal{E}_\pm = \nu_{\sigma\zeta} \pm \sqrt{\nu_{\sigma\zeta}^2 - 1 + 2\varepsilon/hw_H}$ and $\nu_{\sigma\zeta} = \zeta - \sigma/h$. A straightforward integration for the above-cross-point region $\varepsilon > \varepsilon_c$ gives as the exact relation: $\rho_\varepsilon = \rho_{2D}$, while for the below-cross-point region $\varepsilon < \varepsilon_c$ we plot $\rho_\varepsilon/\rho_{2D}$ versus dimensionless energy $2\varepsilon/m\bar{v}^2$ for different fields $h$. Figure 2(b) shows this density of states for different dimensionless magnetic fields. Two points deserve special attention. First, the typical $\varepsilon^{-1/2}$ singularity around $\varepsilon=0$, which occurs for $h=0$, tends to disappears with increasing field. Second, the abrupt step corresponding to the upper ($\sigma=1$) level is shifted with $h$ due to the Zeeman splitting. It should be noted that $\rho_\varepsilon/\rho_{2D} \to 1/2$ for $h>10$ in the low energy region because only the contribution of the lowest ($\sigma=-1$) level takes place.

## IV. NUMERICAL RESULTS

Here we perform numerical calculations based on the simplified consideration outlined in Sec. II B, as well as the self-consistent solution of the eigenstate problem of Sec. II A. The correspondent level-splitting at the Fermi energy level in a selectively doped heterojunction and the densities of states in QWs are described.

### A. Selectively doped heterojunction

The eigenfunction of Eq. (20) for $z>0$ is written through the Airy Ai function, $\mathrm{Ai}[z/l_\perp - (E-\varepsilon_{\sigma\mathbf{p}})/\varepsilon_\perp]$ with $l_\perp = \sqrt[3]{\hbar^2/2m|e|F_\perp}$ and $\varepsilon_\perp = (\hbar/l_\perp)^2/2m$, if the zero boundary condition at $z\to\infty$ is applied. After substitution of this function into the system (22), one obtains the dispersion equation in the form:

$$\det\begin{bmatrix} \mathcal{P}_+ - i\chi\dfrac{\bar{v}p^2 + w_H p_x}{w_\mathbf{p}}\varphi_0^{(a,+1)} & -i\chi\dfrac{w_H p_y}{\bar{v}p_+ + w_H}\varphi_0^{(a,-1)} \\ -i\chi\dfrac{w_H p_y}{\bar{v}p_- + w_H}\varphi_0^{(a,+1)} & \mathcal{P}_- + i\chi\dfrac{\bar{v}p^2 + w_H p_x}{w_\mathbf{p}}\varphi_0^{(a,-1)} \end{bmatrix} = 0. \tag{26}$$

After calculating this determinant and introducing the dimensionless function $K(x) \equiv -\mathrm{Ai}'(x)/\mathrm{Ai}(x)$ one transforms Eq. (26) into

$$\left[\frac{P_o l_\perp}{\hbar} + K\left(\frac{\varepsilon_{+1p} - E}{\varepsilon_\perp}\right) - v_s\frac{\bar{v}p^2 + w_H p_x}{\varepsilon_\perp w_\mathbf{p}}\right] \times \left[\frac{P_o l_\perp}{\hbar} + K\left(\frac{\varepsilon_{-1p} - E}{\varepsilon_\perp}\right) + v_s\frac{\bar{v}p^2 + w_H p_x}{\varepsilon_\perp w_\mathbf{p}}\right] - \left(\frac{v_s w_H p_y}{\varepsilon_\perp w_\mathbf{p}}\right)^2 = 0, \tag{27}$$

where $v_s = \chi\varepsilon_\perp l_\perp/\hbar$ is the spin velocity due to the interface contribution. The spin-dependent dispersion relation, $E_{\sigma\mathbf{p}}$, is given by the roots of this equation.

Let us consider the 2D approach, when $E$ is around the ground energy level, $\varepsilon_o$, determined by the equation: $P_o l_\perp/\hbar + K(-\varepsilon_o/\varepsilon_\perp) = 0$. Expanding $K[(\varepsilon_{\sigma p} - E)/\varepsilon_\perp]$ over $E - \varepsilon_o - \varepsilon_p$ one can transform Eq. (27) into a quadratic equation and the dispersion relation takes the form $E_{\sigma\mathbf{p}} \simeq \varepsilon_o + \varepsilon_p + \sigma\Delta E_\mathbf{p}$, where the splitting $\Delta E_\mathbf{p}$ of the energy spectrum is given by

$$\Delta E_\mathbf{p} = \sqrt{\left(w_\mathbf{p} - \bar{v}_s\frac{\bar{v}p^2 + w_H p_x}{w_\mathbf{p}}\right)^2 + \left(\frac{\bar{v}_s w_H p_y}{w_\mathbf{p}}\right)^2}, \tag{28}$$

with the heterojunction-induced spin velocity, $\bar{v}_s = v_s/K(-\varepsilon_o/\varepsilon_\perp)$, and the internal spin velocity, $\bar{v}$, introduced in Eq. (17). In Fig. 3 we plot these dispersion relations for the same parameters used in Fig. 2(a). As in Fig. 2(a), we have used dimensionless energy and momenta to represent a general case. Comparing Fig. 2(a) with Fig. 3 we can see the effect of the interface contribution as an enhancement of the splitting between parabolas $\sigma = \pm 1$.

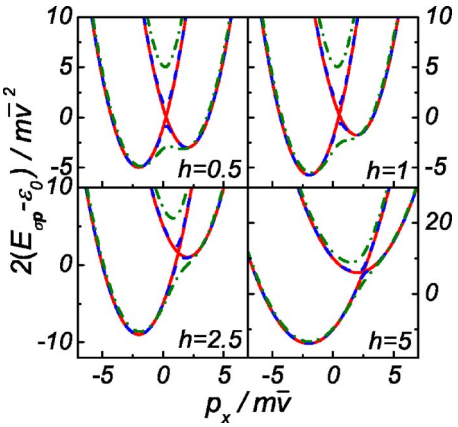


FIG. 3. (Color online) Energy dispersion relations calculated with Eq. (28) for $\bar{v}_s=\bar{v}$ for different magnetic fields $h$. Solid, dashed, and dot-dashed curves correspond to the dimensionless momenta $p_y/m\bar{v}=0$, 0.25, and 1, respectively.

For high electron concentration the approach of Eq. (28) is no longer valid. In order to obtain $E$ for this case we need to solve Eq. (10) together with Eq. (13) by means of a self-consistent approach. To do that we have used the transfer matrix method.[20] Figure 4 shows dispersion relations obtained in this way for $In_{0.75}Al_{0.25}As/In_{0.75}Ga_{0.25}As$ with the electron density $n_{2D}=10^{12}$ cm$^{-2}$, corresponding to a Fermi energy $\varepsilon_F\simeq 130$ meV, which slightly depends on magnetic field [see Fig. 4(b)]. Using the standard parameters[21] one obtains $\chi\simeq 0.09$ and $\bar{v}=1.78\times 10^6$ cm/s, so that dimensionless field $h=1$ corresponds to $H=0.15$ T. Thus we can compare the panel for $h=1$ in Fig. 3 with the left upper panel in Fig. 4(a). We can see that numerically calculated results show a similar behavior than approximation (28), although, for the material under consideration, the shift along momentum is smaller in Fig. 4(a). A visible spin splitting [up to 10 meV, see Fig. 4(b)] takes place at the Fermi energy. Moreover, the anisotropy of dispersion relations appears to be essential if $H>1.5$ T.

The spin splitting of the dispersion relations at Fermi energy is directly connected to the SdH oscillations. Since $\Delta E_{\mathbf{p}}$ is nearly isotropic over the $\mathbf{p}$-plane, we have also calculated $\Delta E=\Delta E_{\mathbf{p}}|_{p=p_F}$ for different magnetic fields, see Fig. 5. Following Refs. 12 and 13 the spin splitting is related to the modulation of the SdH oscillation amplitude according to $\cos(\pi m\Delta E/\hbar|e|H)$. For the above-discussed structure, experimental value[13] is $\Delta E=11.4$ meV for $H=0.8$ T, which corresponds to $\Delta E=9.96$ meV, calculated numerically for the same magnetic field and $n_{2D}$. Figure 5 shows a two-time enhancement of $\Delta E$ for $\chi=0.09$ in comparison with the case $\chi=0$. In addition, we have included here $\Delta E$ versus $H$ for the $In_{0.52}Al_{0.48}As/In_{0.53}Ga_{0.47}As$ structure which was only investigated under transverse magnetic fields in Ref. 12. The calculation also demonstrates an essential enhancement of the spin splitting if $\chi\neq 0$. Thus interface contributions should be detectable through the SdH oscillations measurements.

### B. QW under field $F_\perp$

Next, we consider the nondoped symmetric QW (with $P_\pm=P_o$ and $\chi_\pm=\chi$) subjected to a transversal field $F_\perp$, when

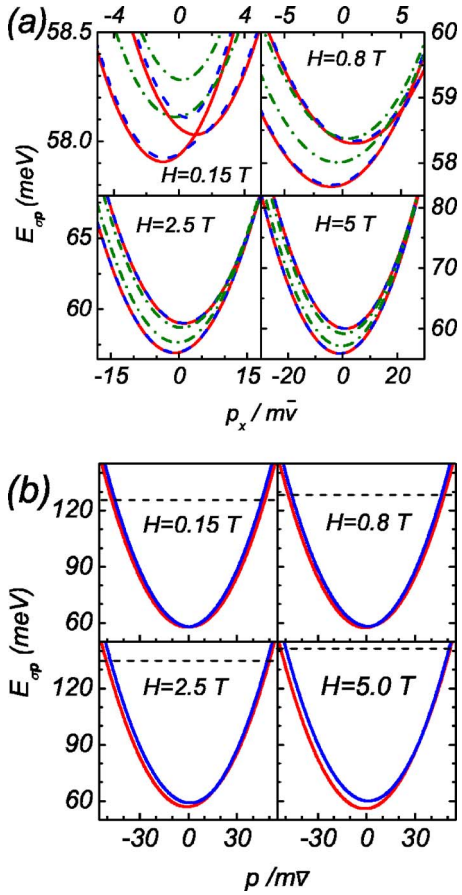


FIG. 4. (Color online) (a) Dispersion relations for $In_{0.75}Al_{0.25}As/In_{0.75}Ga_{0.25}As$ heterostructure with $n_{2D}=10^{12}$ cm$^{-2}$ calculated numerically for different magnetic fields $H$. Solid line: $p_y=0$. Dashed line: $p_y=m\bar{v}$. Dot-dashed line: $p_y=2.5m\bar{v}$. (b) The same as in (a) for an energy scale up to the correspondent Fermi energy (dashed lines).

the eigenstate functions of Eq. (20), $\varphi_z^{(a,b)}$, are written through the Ai- and Bi-functions. The system (24) gives the dispersion relations equation as the determinant of a $4\times 4$ matrix, which differs from Eq. (26) due to the replacement of $\mathcal{P}_\pm$ and $\varphi_o^\pm$ by the $2\times 2$ matrices:

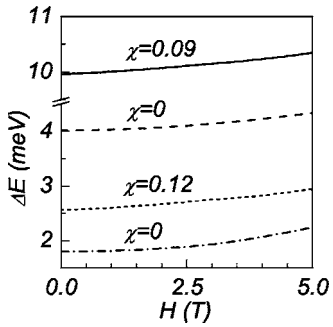


FIG. 5. Level splitting energy, $\Delta E$, vs magnetic field for $In_{0.75}Al_{0.25}As/In_{0.75}Ga_{0.25}As$ (solid and dashed curves) and $In_{0.52}Al_{0.48}As/In_{0.53}Ga_{0.47}As$ (dotted and dot-dashed curves) heterostructures. $\chi$ are marked near the curves.

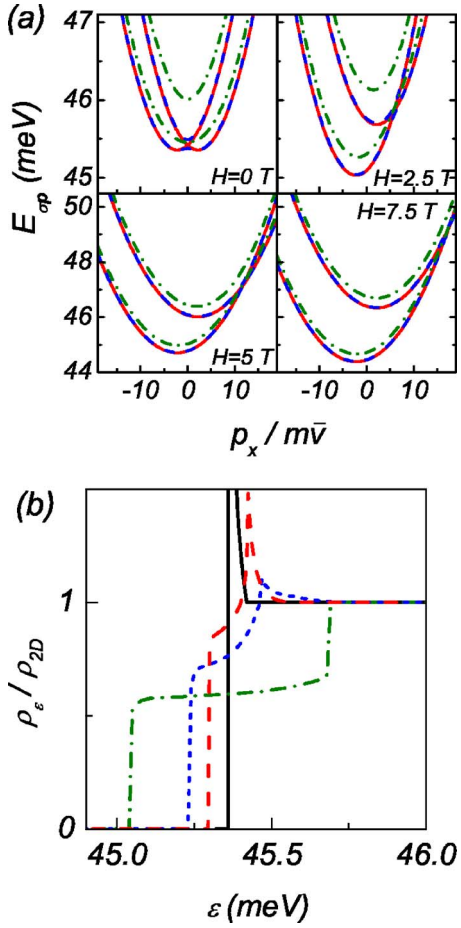


FIG. 6. (Color online) (a) Dispersion laws for InGaAs/InAlAs QW under different magnetic fields. $p_y=0$ (solid line) and $p_y=m\bar{v}$ (dashed line). (b) Density of states for $H=0$ $T$ (solid line), 0.5 $T$ (dashed line), 1 $T$ (dotted line), and 2.5 $T$ (dot-dashed line).

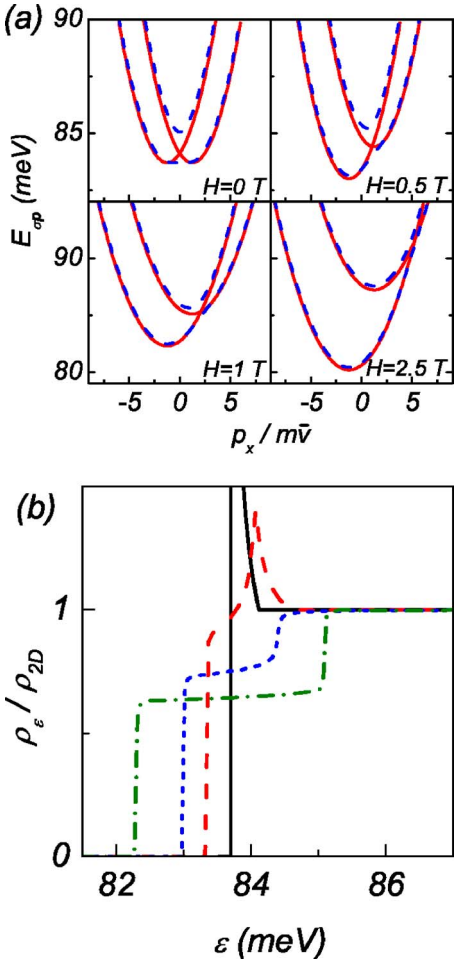


FIG. 7. (Color online) (a) Dispersion relations for InSb/InAlSb QW under different magnetic fields. $p_y=0$ (solid line) and $p_y=m\bar{v}$ (dashed line). (b) Density of states for $H=0$ $T$ (solid line), 0.25 $T$ (dashed line), 0.5 $T$ (dotted line), and 1 $T$ (dot-dashed line).

$$\hat{\mathcal{P}}_\sigma = \begin{bmatrix} \mathcal{P}_+^{(a\sigma)} & \mathcal{P}_+^{(b\sigma)} \\ \mathcal{P}_-^{(a\sigma)} & \mathcal{P}_-^{(b\sigma)} \end{bmatrix}, \quad \hat{\varphi}_\sigma = \begin{bmatrix} \varphi_{d/2}^{(a\sigma)} & \varphi_{d/2}^{(b\sigma)} \\ \varphi_{-d/2}^{(a\sigma)} & \varphi_{-d/2}^{(b\sigma)} \end{bmatrix}, \tag{29}$$

where $\mathcal{P}_\pm^{(k\sigma)} \equiv (\hat{p}_z \varphi_z^{(k,\pm 1)})_{z=\pm d/2} \mp i P_o \varphi_{\pm d/2}^{(k,\pm 1)}$. Once again, after the expansion near the ground energy, $\varepsilon_o$, one can transform the determinant in a similar way to transformations of Eqs. (26) and (27). Numerical solutions of these equations for InGaAs- and InSb-based QWs are represented in Figs. 6(a) and 7(a). We have considered 100 Å wide InGaAs- and InSb-based QWs using the parameters of Refs. 21 and 22. We have also applied a field of 120 kV/cm, which corresponds to spin velocity $\bar{v}=1.04\times10^6$ cm/s, for the InGaAs QW, and a field of 100 kV/cm, spin velocity $\bar{v}=8.2\times10^6$ cm/s, for the InSb.

Comparing Figs. 6(a) and 7(a) with Fig. 4 we can see that, for similar spin velocities and magnetic fields, the splitting between levels is bigger whereas the shift in the $p_x$ direction is smaller for the QW case with respect to the selectively doped structure. Thus the effect of interface contribution seems to be more pronounced for the QW case. This effect is enhanced as the width of the wells diminishes. Due to the greater spin velocities of InGaAs and InSb-based QWs, caused by the different effective masses and energy gaps, the use of lesser magnetic fields is necessary to get a similar effect. Both for QWs and selectively doped structures, interface contributions are opposite to the intrinsic spin-orbit coupling effect.

Since the density of states is proportional to the PLE intensity,[7,19] as shown in Eq. (16), it is interesting to study the shape of $\rho_\varepsilon$, shown in Figs. 6(b) and 7(b). The effect of the interfaces is manifested in $\rho_\varepsilon$ as a delay in the quenching of the $\varepsilon^{-1/2}$-singularity corresponding to the zero-field case. Although the singularity no longer exists for $H\neq0$, a peak still remains at the energy value of the bands anticrossing. For the case which includes interface contributions, this peak gets wider and $\rho_\varepsilon$ tends slower to $\rho_{2D}$ for the high energy limit. Thus the PLE technique is of great interest to analyze the interface contributions.[23] It should be noticed that the two-step structure, with $\rho_\varepsilon/\rho_{2D}$ equal to 1/2 or 1, takes place for magnetic fields beyond 5 T.

## V. CONCLUSION

In this paper we have examined the electron states in narrow-gap nonsymmetric heterostructures under an in-plane

magnetic field. The eigenstate problem was formulated in the framework of the three-band Kane model with nonsymmetric boundary conditions. We have found that the mechanisms of mixing between the Zeeman term in the Hamiltonian and the two kinds of spin-orbit coupling contributions (from a slow field and from heterojunctions) are essentially different. Numerical estimates for typical parameters of InGaAs/InAlAs and InSb/InAlSb structures demonstrate the essential magnetoinduced modifications of the energy spectra under magnetic field strength of the order of Tesla.

Let us discuss some possibilities for the experimental verification of the energy spectra modifications obtained here. The magnetotransport measurements of SdH oscillations under nearly in-plane magnetic fields[12,13] (when a quasiclassic quantization of the dispersion relations for the transverse component of the magnetic field is possible) provide direct information about in-plane magnetoinduced modifications of electron energy spectra. The results of Sec. IV A are in agreement with Ref. 13 but more measurements (for different in-plane fields and concentrations) are necessary in order to separate the intrinsic and junction-induced contributions. Another way of looking for these peculiarities of energy spectra is the midinfrared PLE spectroscopy[23] when interband transitions are modified under in-plane magnetic field. PLE intensity provides direct information of the energy spectra because it is directly connected to the density of states, as mentioned above. A comparison between SdH oscillations and PLE measurements with a precision about 1 meV (it should be possible for a high-quality structure) provides more data on mechanisms of spin-orbit interaction in narrow-gap structures.

Next, we list some assumptions made in the calculations. The following standard simplifications of the energy band spectra have been used: (a) the neglect of the nonparabolicity effect is correct for energy values smaller than $\varepsilon_g$; (b) the three-band Kane model is valid for the narrow-gap structures under consideration; and (c) the weak underbarrier penetration is described by the boundary conditions (8) and (12) for energy values smaller than $\Delta\varepsilon_c$. An analysis taking into account the above factors does not change the structure of the eigenstate problem formulated in Sec. II B, thus the main conclusions of the paper about interplay between different contributions to spin-splitting still remain valid. In addition, in Eq. (9) we have neglected the effect of the magnetic field on the level quantization under the condition $\hbar\omega_c \ll \bar{v}\hbar/\bar{d}$, which is satisfied for the narrow-width structures under consideration. The assumption of the effective transverse field $F_\perp$ gives us correct estimations for the magnetoinduced modifications of the dispersion relations and more detailed numerical calculations are needed for the concrete heterostructures under consideration.

Thus we have shown the essential modifications of the electron energy spectra in nonsymmetric narrow-gap QWs under in-plane magnetic fields. We suggest that measurements of the magnetoinduced contributions to optical and transport properties would be a useful method for an experimental verification of the heterojunction-induced contributions to the spin-orbit interaction in the narrow-gap heterostructures under investigation.

## ACKNOWLEDGMENT

This work has been supported in part by Ministerio de Educación y Ciencia (Spain) and FEDER under the project FIS2005-01672.

*Electronic address: ajhernan@ull.es
†Electronic address: ftvasko@yahoo.com

[1] W. Zawadzki and P. Pfeffer, Semicond. Sci. Technol. **19**, R1 (2004).
[2] Y. Yafet, Solid State Phys. **14**, 1 (1963); V. F. Gantmakher and I. B. Levinson, *Carrier Scattering in Metals and Semiconductors* (North-Holland, Amsterdam, 1987).
[3] G. Dresselhaus, Phys. Rev. **100**, 580 (1955).
[4] E. I. Rashba, Sov. Phys. Solid State **2**, 1109 (1960); E. I. Rashba and V. I. Sheka, *ibid.* **3**, 1718 (1961).
[5] M. I. Dyakonov, and V. Y. Kachorovskii, Sov. Phys. Semicond. **20**, 110 (1986).
[6] F. T. Vasko, JETP Lett. **30**, 360 (1979).
[7] F. T. Vasko and A. V. Kuznetsov, *Electronic States and Optical Transitions in Semiconductor Heterostructures* (Springer, New York, 1999); A. V. Rodina and A. Yu. Alekseev, Phys. Rev. B **73**, 115312 (2006); W. Yang and K. Chang, *ibid.* **73**, 113303 (2006).
[8] A. Darr, J. P. Kotthaus, and T. Ando, *Proceedings 13th Int. Conf. Phys. Semicond.*, edited by F. G. Fumi (North-Holland, Amsterdam, 1976), p. 774; T. Ando, A. B. Fowler, and F. Stern, Rev. Mod. Phys. **54**, 437 (1982); D. A. Romanov, Phys. Solid State **35**, 717 (1993).
[9] F. T. Vasko and N. A. Prima, Sov. Phys. Solid State **25**, 331 (1983).
[10] F. T. Vasko and O. Keller, Phys. Rev. B **58**, 15666 (1998).
[11] P. Pfeffer and W. Zawadzki, Phys. Rev. B **59**, R5312 (1999); Y. Lin, T. Koga, and J. Nitta, *ibid.* **71**, 045328 (2005).
[12] B. Das, D. C. Miller, S. Datta, R. Reifenberger, W. P. Hong, P. K. Bhattacharya, J. Singh, and M. Jaffe, Phys. Rev. B **39**, 1411 (1989); J. Luo, H. Munekata, F. F. Fang, and P. J. Stiles, *ibid.* **38**, 10142 (1988).
[13] T. Kita, Y. Sato, S. Gozu, and S. Yamada, Physica B **298**, 65 (2001).
[14] Y. V. Pershin, J. A. Nesteroff, and V. Privman, Phys. Rev. B **69**, 121306(R) (2004).
[15] M.-C. Chang, Phys. Rev. B **71**, 085315 (2005).
[16] E. O. Kane, J. Phys. Chem. Solids **1**, 249 (1957); G. Bastard, Phys. Rev. B **24**, 5693 (1981).
[17] E. A. de Andrada e Silva, G. C. La Rocca, and F. Bassani, Phys. Rev. B **55**, 16293 (1997).
[18] The final Schrödinger equation (10) and corresponding boundary conditions (8) and (12) do not change after taking into account the stress-induced splitting of $v$-band extrema and such a revision of the parameters changes the numerical estimation only slightly but the main results are the same.

[19] P. Y. Yu and M. Cardona, *Fundamentals of Semiconductors* 3rd ed. (Springer-Verlag, Berlin, 2001).

[20] A. Hernández-Cabrera, P. Aceituno, and F. T. Vasko, Phys. Rev. B **60**, 5698 (1999).

[21] Following Refs. 11–13 and I. Vurgaftman, J. R. Meyer, and L. R. Ram-Mohan, J. Appl. Phys. **89**, 5815 (2001), we use the data for the $In_{0.75}Al_{0.25}As/In_{0.75}Ga_{0.25}As$ structure: $m=0.035m_e$, $m_b=0.048m_e$, where $m_e$ is the electron mass, factor $g=14.29$, permittivity $\epsilon=13.9$, $\Delta E_c=246$ meV, $\Delta E_v=105.5$ meV, and $\varepsilon_g=604$ meV. For the $In_{0.52}Al_{0.48}As/In_{0.53}Ga_{0.47}As$ structure: $m=0.041m_e$, $m_b=0.0754m_e$, factor $g=12.2$, permittivity $\epsilon=13.9$, $\Delta E_c=498$ meV, $\Delta E_v=197$ meV, and $\varepsilon_g=813$ meV. For the $In_{0.8}Al_{0.2}As/In_{0.52}Ga_{0.48}As$ structure: $m=0.041m_e$, $m_b=0.2m_e$, factor $g=-4.5$, permittivity $\epsilon=13.9$, $\Delta E_c=1268.6$ meV, $\Delta E_v=493.4$ meV, and $\varepsilon_g=813$ meV.

[22] National Compound Semiconductor Roadmap: InSb, http://www.onr.navy.mil/sci_tech/information, 2005. Data for $InSb/In_{0.8}Al_{0.2}Sb$ are $m=0.0142m_e$, $m_{\pm}=0.0234m_e$, $\Delta E_c=220.0$ meV, $\Delta E_v=99.5$ meV, $\varepsilon_g=246.6$ meV, $g=-48.5$, and $\epsilon=16.1$.

[23] T. A. Liu, K. F. Huang, C. L. Pan, S. Ono, H. Ohtake, and N. Sarukura, Jpn. J. Appl. Phys., Part 2 **40**, L681 (2001).